Monthly Notices of the ROYAL ASTRONOMICAL SOCIETY

MNRAS **545,** 1–14 (2026) https://doi.org/10.1093/mnras/staf2062
Advance Access publication 2025 November 21

Characterizing EP241107a: multiwavelength observations of an *Einstein Probe*-detected fast X-ray transient

D. Eappachen [1★] A. Balasubramanian [1] Vishwajeet Swain [2] G. C. Anupama [1] D. K. Sahu [1] V. Bhalerao [2] T. Ahumada [3] I. Andreoni [4] Sudhanshu Barway [1] J. Carney [4] J. Freeburn [4] M. M. Kasliwal [3] Tanishk Mohan [2] A. C. Rodriguez [5] and G. Waratkar [2,3]

[1]*Indian Institute of Astrophysics, II Block, Koramangala, Bengaluru, Karnataka 560034, India*
[2]*Department of Physics, Indian Institute of Technology Bombay, Powai 400 076, India*
[3]*Cahill Center for Astrophysics, California Institute of Technology, MC 249-17, 1216 E California Boulevard, Pasadena, CA 91125, USA*
[4]*Department of Physics and Astronomy, University of North Carolina at Chapel Hill, Chapel Hill, NC 27599-3255, USA*
[5]*Center for Astrophysics | Harvard & Smithsonian, 60 Garden Street, Cambridge, MA 02138, USA*

Accepted 2025 November 6. Received 2025 November 4; in original form 2025 September 30

ABSTRACT

Fast X-ray transients (FXTs) represent a new class of highly luminous transients in soft X-rays (∼0.3–10 keV) associated with violent astrophysical processes. They manifest as short, singular flashes of X-ray photons with durations lasting from minutes to hours. Their origin remains unclear, and they have been associated with various progenitor mechanisms. The newly launched X-ray survey, *Einstein Probe* (EP), is revolutionizing this field by enabling the discovery and immediate follow-up of FXTs. Here, we present the multiwavelength observations of EP-discovered FXT EP241107a and the discovery of its radio counterpart. Comparison of the optical and radio observations of EP241107a and its host properties with other extragalactic transients suggests a gamma-ray burst (GRB) origin. Through our afterglow modelling, we infer the GRB jet properties for EP241107a, yielding a jet of the isotropic-equivalent kinetic energy $E_{\rm K,iso} \sim 10^{51}$ erg, with a half opening angle $\theta_c \approx 15^\circ$, viewed at an angle of $\theta_{\rm obs} \approx 9^\circ$. We also evaluate EP241107a in the landscape of both EP-discovered FXTs as well as the FXTs discovered from *Chandra*, *XMM–Newton,* and *Swift*-X-ray Telescope.

Key words: stars: jets – radio continuum: transients – gamma-ray bursts.

1 INTRODUCTION

Fast X-ray transients (FXTs) are bursts in soft X-rays (∼0.3–10 keV) with durations ranging from a few hundred to 10^4 s. Before the launch of *Einstein Probe* (EP; W. Yuan et al. 2022), roughly 95 per cent of the FXTs were discovered through searches in X-ray archival data, especially from *Chandra* (P. G. Jonker et al. 2013; A. Glennie et al. 2015; F. E. Bauer et al. 2017; Y. Q. Xue et al. 2019; J. Quirola-Vásquez et al. 2022; D. Lin et al. 2022; J. Quirola-Vásquez et al. 2023; D. Eappachen et al. 2023) and *XMM–Newton* archives (D. Alp & J. Larsson 2020; G. Novara et al. 2020; I. Pastor-Marazuela et al. 2020). Most FXTs were identified and reported months or years after the bursts, thereby lacking prompt follow-ups and, therefore, no multiwavelength counterparts were detected except in one case. It was in the case of SN2008D, where a serendipitous detection of the FXT associated with a supernova shock breakout (SN SBO) was reported by A. M. Soderberg et al. (2008) using *Swift*-X-ray Telescope (XRT). In the absence of multiwavelength counterparts, significant efforts have been made to study the associated host galaxies of the FXTs, thereby constraining their origin (e.g. Y. Q. Xue et al. 2019; D. Lin et al. 2022; D. Eappachen et al. 2022, 2024; D. Ibrahimzade et al. 2025; A. Inkenhaag et al. 2024; J. Quirola-Vásquez et al. 2025).

FXTs represent a heterogeneous and still poorly understood class of X-ray transients whose diversity implies that no single progenitor model can adequately account for their origin. Major progenitor mechanisms include (i) an SN SBO where an X-ray flash is produced as the shock wave from a supernova crosses the surface of the star (A. M. Soderberg et al. 2008; E. Waxman & B. Katz 2017; J. A. Goldberg, Y.-F. Jiang & L. Bildsten 2022); (ii) a white dwarf (WD) –intermediate-mass black hole (IMBH) tidal disruption event (TDE) which could produce bursts in X-rays that last for shorter timescales compared to supermassive black hole TDE (M. MacLeod et al. 2016; K. Maguire et al. 2020); (iii) a long gamma-ray burst (lGRB) association where X-ray emission is produced when a mildly relativistic cocoon jet breaks the surface of a massive progenitor star (E. Ramirez-Ruiz, A. Celotti & M. J. Rees 2002; E. Nakar & T. Piran 2017); or (iv) an X-ray emission from a magnetar formed as a result of a binary neutron star merger (BNS; B. D. Metzger & A. L. Piro 2014; H. Sun, B. Zhang & H. Gao 2017). H. C. I. Wichern et al. (2024) suggest a region of parameter space where the observational properties of off-axis GRB afterglows align with those of FXTs.

EP is revolutionizing the field of FXTs by discovering and reporting X-ray transients in the X-ray band of 0.5–4 keV within a few minutes/hours of the FXTs, enabling prompt follow-up. Follow-

★ E-mail: deepak.eappachen@iiap.res.in

up of some of these FXTs reveals an extragalactic nature: for instance, EP240315a (J. H. Gillanders et al. 2024; A. J. Levan et al. 2024; Y. Liu et al. 2025) at a redshift of $z = 4.859$ is consistent with a lGRB (J. H. Gillanders et al. 2024; A. J. Levan et al. 2024; R. Ricci et al. 2025). Recent multiwavelength observations of the EP-FXTs provide further evidence supporting multiple origins (J. H. Gillanders et al. 2024; A. J. Levan et al. 2024, 2025; J. N. D. Dalen et al. 2025; S. Srivastav et al. 2025; J. C. Rastinejad et al. 2025; G. P. Srinivasaragavan et al. 2025; R. A. J. Eyles-Ferris et al. 2025; P. G. Jonker et al. 2025).

One of the well-studied EP-discovered FXTs is the recently reported EP240414a (J. N. D. Dalen et al. 2025; S. Srivastav et al. 2025; H. Sun et al. 2025; J. S. Bright et al. 2025) which was found to be located in a massive galaxy at a redshift of $z = 0.401$ at a projected distance of 25.7 kpc from the galactic centre. The optical light curve of the counterpart shows three different components which are suggested to be due to the initial dominant contribution from a thermal cocoon emission, followed by the circumstellar medium-interaction and the third phase dominated by the SN radioactive decay (J. N. D. Dalen et al. 2025). The fast rise time in the second phase of the light curve of the optical counterpart of EP240414a along with the extremely blue optical spectrum is similar to properties seen in Luminous Fast Blue Optical Transients (LFBOTs; S. J. Prentice et al. 2018). At later time-scales, the spectrum shows similar features to that of broad-lined Type Ic SNe, suggesting a collapsar origin, although no gamma-ray counterpart has been detected. Another EP-FXT EP241021a (M. Busmann et al. 2025; G. Gianfagna et al. 2025; S. Xinwen et al. 2025; M. Yadav et al. 2025; G.-L. Wu et al. 2025) also shows a very similar optical afterglow light curve to that of EP240414a. However, for EP241021a, no features of an associated SN were found. The detection of the radio counterpart and the apparent absence of a gamma-ray counterpart indicate that a low luminosity GRB (LL-GRB) could have gone undetected or an off-axis or choked jet could be responsible for the radio emission. In addition to both the above-discussed EP-FXTs, an intensive follow-up campaign to search for the counterpart of EP240408a was reported (B. O'Connor et al. 2025b). However, deep optical and radio observations resulted in non-detections of the transient. B. O'Connor et al. (2025b) favour a peculiar GRB or jetted WD-IMBH TDE at high redshift ($z \gtrsim 1$), though neither perfectly explains the observations. This highlights the diverse range of transients that EP is unveiling, including FXTs with distinct origins. The redshift distribution of these EP-discovered FXTs offers valuable insights into their possible progenitor mechanisms (B. O'Connor et al. 2025a).

In this paper, we report our multiwavelength follow-up observations of the FXT EP241107a. The FXT EP241107a was detected by the Wide-field X-ray Telescope (WXT) on board the EP, at 2024-11-07T14:10:23 UTC (H. Zhou et al. 2024). EP241107a trigger flux is estimated to be around 10^{-10} erg cm^2 s^{-1}in 0.5−4 keV band. The follow-up X-ray telescope (FoXT),[1] on EP carried out follow-up observations about five minutes later, which detected an X-ray source at RA = $02^h20^m02.04^s$, Dec. = $+03^\circ$ 19′ 58.44″ with an uncertainty of about 10″. The follow-up observations from the Al-Khatim Observatory detected and reported the detection of an optical counterpart at RA and Dec. $02^h20^m02.45^s$, $+03^\circ$ 20′ 02.2″ in the I_c band at a magnitude of 17.85±0.18 (M. Odeh et al. 2024a). Though reported later, the earliest optical counterpart detection for EP241107a was by Chinese Ground Follow-up Telescope of *SVOM* mission, which detected the counterpart a magnitude of 17.12 ± 0.10 in i band, starting the observations just ∼ 5.5 min after the EP-WXT trigger (Z. Kang, C. Wu & L. Xin 2024).

We use our multiwavelength observations of the transient counterpart, along with publicly available data, combined with our afterglow and host modelling, to derive constraints on the nature of EP241107a. Throughout the paper; we assume a flat Lambda-cold dark matter cosmology, with *Hubble* constant $H_0 = 67.8 \pm 0.9$ km s^{-1}Mpc^{-1} and matter density parameter $\Omega_m = 0.308 \pm 0.012$ (Planck Collaboration XIII 2016). Magnitudes are quoted in the AB system.

2 OBSERVATIONS AND ANALYSIS

2.1 GROWTH-India Telescope

The GROWTH-India Telescope (GIT; H. Kumar et al. 2022), located at the Indian Astronomical Observatory (IAO), Hanle, India, is a 0.7 m robotic telescope with a 0.7° field of view and is dedicated to observing the transient sky. We observed the field of EP241107a in Sloan g', r', and i' filters within ∼3.55 h after EP-WXT trigger. We utilized a PYTHON-based pipeline (H. Kumar et al. 2022) to obtain the photometry, making use of the Panoramic Survey Telescope And Rapid Response System Data Release 2 (Pan-STARRS DR2; K. C. Chambers et al. 2016) catalogue for photometric and astrometric calibration.

An optical counterpart was detected at an r'-filter magnitude of 19.42 ± 0.07 at the same RA and Dec. as reported by M. Odeh, S. Alshamsi & N. M. Pattani (2024b). The GIT detection image of EP241107a is shown in left panel of Fig. 1. We obtained the photometry of the counterpart to EP241107a in two more epochs, and the magnitudes and upper limits are given in Table 1.

2.2 Himalayan-Chandra Telescope

We observed the field of EP241107a using the Himalaya Faint Object Spectrograph Camera (HFOSC) mounted at the 2-m Himalayan Chandra Telescope (HCT) of the IAO, Hanle, India. The observations started at 2024-11-09T20:54:24.03 UT in r' filter. We used IRAF (D. Tody 1986) for bias and flat-field correction, whereas for cosmic removal, L.A. Cosmic (P. G. Dokkum 2001) was employed. A total of 540-s exposure was obtained, and we used the IRAF IMCOMBINE task for stacking. We applied the astrometric correction to the stacked image using astrometry.net[2] (D. Lang et al. 2010)

At ∼2.28 d after the trigger, we did not find any associated counterpart for EP241107a in the HCT r' image. The photometric calibration of the image was done using stars from the Pan-STARRS DR2 catalogue data (K. C. Chambers et al. 2016). We deduced a 5σ optical upper limit of 22.5 in r' filter 2.28 d after the EP-trigger.

2.3 The 4.1-m Southern Astrophysical Research Telescope

With the Goodman High Throughput Spectrograph's red camera, mounted on the Southern Astrophysical Research (SOAR; J. C. Clemens, J. A. Crain & R. Anderson 2004) telescope, the location of the optical counterpart to EP241107a was observed (PI: Andreoni; J. Freeburn, I. Andreoni & J. Carney 2024) ∼3.5 d after the X-ray transient. Difference imaging was conducted with saccadic fast Fourier transform (L. Hu et al. 2022), using templates from the

[1] EP follow-up X-ray telescope is conventionally named EP-FXT. However, to avoid confusion with fast X-ray transients (FXT), we are using the EP-FoXT acronym for the EP follow-up X-ray telescope.

[2] https://nova.astrometry.net/upload

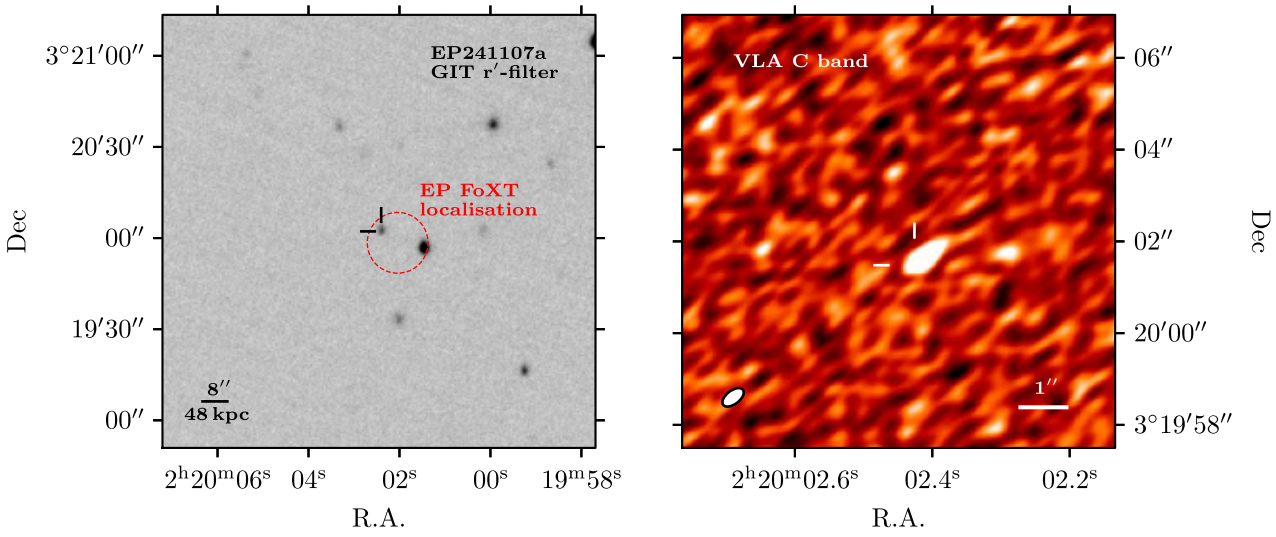

Figure 1. The location of the counterparts to EP241107a in optical and radio bands is shown. The left panel shows the GIT r'-filter image of the field of EP241107a, 0.165 d after the EP-trigger. The EP-FoXT uncertainty region of 10 arcsec is marked with a dashed circle, while the optical counterpart of EP241107a is marked with lines. The VLA *C*-band image of the field of EP241107a is shown in the right panel. The VLA beam size for this observation is given in the bottom left of the image. Note that the scales of the optical and radio images are different.

DECam Legacy Survey (A. Dey et al. 2019). The optical counterpart was not detected in these observations with 5σ upper limits of $g = 22.4$, $r = 22.9$, and $i = 22.7$. The photometric light curve of EP241107a is shown in Fig. 2.

2.4 Keck LRIS

Spectroscopic observation of EP241107a was carried out on the Keck I telescope, starting at 2024-11-08T08:34:17.9 UT using the Low-Resolution Imaging Spectrometer (LRIS; J. B. Oke et al. 1995). Using the 600 ℓ mm^{-1} blue grism ($\lambda_{\rm blaze} = 4000$ Å), the 400 ℓ mm^{-1} red grating ($\lambda_{\rm blaze} = 8500$ Å), the 5600 Å dichroic, and the 1 arcsec slit we obtained a 900 s observation covering the full optical window at moderate resolving power, $R \equiv \lambda/\Delta\lambda \approx 1500$ for objects filling the slit. We used BD+284211 observed with the same instrument configuration for flux calibration. We used the code LPIPE to reduce and flux calibrate the spectrum (D. A. Perley 2019).

In the optical counterpart spectrum of EP241107a (Fig. 3), we identified the emission lines associated with the underlying host galaxy, namely Hα λ6564.6,[3] Hβ λ4862.7, [O II] λ3728.5, and [O III] λ4960.3, 5008.2. We fitted multiple Gaussians to the emission line using the LMFIT[4] package and obtained the best-fitting central wavelengths and their associated errors. We infer a redshift of z= 0.457 $\pm$ 0.003 for EP241107a.

2.5 Karl G. Jansky Very Large Array Radio Observations

Under our approved Karl G Jansky Very Large Array (VLA) proposal 24B-492 (PI: Balasubramanian), we obtained observations of the field of EP241107a in the *X* band (central frequency of 10 000 MHz) and in the *C* band (central frequency of 6000 MHZ) on 2024 November 24 and December 01, respectively. The raw data weres calibrated using the automated CASA VLA pipeline (version 6.5.4.9) and imaged along with self-calibration using an automated script.[5] We detect a point source-like counterpart to EP241107a in both the frequency bands. Within 10 arcsec of the radio detection, we did not find any existing radio source in the master radio catalogue.[6] This re-affirms that the radio detection is indeed associated with EP241107a. To obtain the flux density of the detected source, we use the CASA task IMFIT and list the peak flux density and error values for the point source in Table 1. The *C*-band image is shown in Fig. 1 (right panel).

2.6 uGMRT Radio Observations

We obtained upgraded Giant Metrewave Radio Telescope (uGMRT) observations of the field of EP241107a in two frequency bands – band 4 (central frequency 750 MHz, bandwidth 400 MHz) and band 5 (central frequency 1260 MHz, bandwidth 400 MHz), on 2024 December 20 and 17, respectively (ddtC404, PI: Eappachen). The raw data were downloaded in the FITS format and converted to the CASA (CASA Team et al. 2022) measurement set format. Then, the data were calibrated and imaged using the automated continuum imaging pipeline CASA-CAPTURE (R. Kale & C. H. Ishwara-Chandra 2021). Eight rounds of self-calibration were done within each pipeline run. We do not detect a significant radio source in the position of EP241107a. We compute the 3 σ upper limits calculated from a large region centred on the source in the residual image and list the values in Table 1.

3 MODELLING

3.1 Modelling the gamma-ray burst afterglow with AFTERGLOWPY

We fit the multiwavelength observations of EP241107a using the publicly available semi-analytical package AFTERGLOWPY (G. Ryan et al. 2020) and EMCEE (D. Foreman-Mackey et al. 2013) code in

[3]Rest wavelengths of the lines in vacuum are from https://classic.sdss.org/dr6/algorithms/linestable.html.
[4]https://lmfit.github.io/lmfit-py/
[5]https://science.nrao.edu/facilities/vla/data-processing/pipeline/VIPL654
[6]https://heasarc.gsfc.nasa.gov/w3browse/master-catalog/radio.html

Table 1. A journal of optical and radio observations of EP241107a used in this paper.

(a) The uGMRT and VLA radio observations of EP241107a

Date and time (UT)	ΔT	Telescope	Frequency (MHz)	Flux density (μJy)
2024-11-24T00:54:58.0	16.45	VLA	10 000	232 ± 9
2024-12-01T00:38:08.0	23.44	VLA	6000	207 ± 8
2024-12-17T16:39:48.6	40.10	uGMRT	1265	< 72
2024-12-20T14:43:24.2	43.02	uGMRT	648	< 255

(b) Optical photometric observations of EP241107a

UT (start)	ΔT (d)	Telescope/Instrument	Optical band	Magnitude	Error	Reference
2024-11-07 00:05:45.600	0.004	Chinese Ground Follow-up Telescope	*i*	17.12	0.10	Z. Kang et al. (2024)
2024-11-07 01:43:40.800	0.072	Al-Khatim Observatory	*Ic*	17.85	0.18	M. Odeh et al. (2024b)
2024-11-07 01:45:07.200	0.073	Al-Khatim Observatory	*Ic*	17.95	0.19	M. Odeh et al. (2024b)
2024-11-07 03:13:40.800	0.095	Al-Khatim Observatory	*Ic*	18.11	0.24	M. Odeh et al. (2024b)
2024-11-07 04:41:25.600	0.116	Al-Khatim Observatory	*Ic*	18.48	0.25	M. Odeh et al. (2024b)
2024-11-07 16:07:26.667	0.165	GIT	*r*	19.45	0.22	This work
2024-11-07 18:23:24.333	0.176	GIT	*g*	19.99	0.05	This work
2024-11-07 18:39:20.667	0.187	GIT	*i*	19.17	0.06	This work
2024-11-07 18:49:55.200	0.210	1-m Las Cumbres Observatory	*i*	19.40	0.10	W. X. Li et al. (2024)
2024-11-07 22:02:52.000	0.263	Fraunhofer Telescope Wendelstein	*r*	19.65	0.01	M. Busmann, D. Gruen & B. O'Connor (2024)
2024-11-07 22:02:52.000	0.263	Fraunhofer Telescope Wendelstein	*i*	19.40	0.01	M. Busmann et al. (2024)
2024-11-07 22:02:52.000	0.263	Fraunhofer Telescope Wendelstein	*J*	18.71	0.01	M. Busmann et al. (2024)
2024-11-07 22:41:42.667	0.295	1.93m OHP	*r*	19.80	0.05	C. Adami et al. (2024)
2024-11-07 21:28:45.000	0.304	GIT	*r*	19.68	0.21	This work
–	0.67	KAIT	*R*	20.50	0.1	W. Zheng et al. (2024)
2024-11-08 14:13:50.667	1.002	GIT	*i*	>20.36	–	This work
2024-11-08 14:45:12.667	1.024	GIT	*g*	>21.68	–	This work
2024-11-08 14:52:57.556	1.030	GIT	*r*	21.59	0.25	This work
2024-11-08 17:53:52.000	1.024	1-m LOT Lulin Observatory	*r*	21.50	0.32	A. K. H. Kong et al. (2024)
2024-11-08 18:51:56.750	1.196	GIT	*r*	21.51	0.25	This work
2024-11-08 20:47:08.583	1.276	GIT	*i*	>21.16	–	This work
2024-11-09 20:54:24.031	2.281	HCT/HFOSC	*r*	>22.5	–	This work
2024-11-10 15:30:05.667	3.055	GIT	*r*	>21.43	–	This work
2024-11-10 16:07:51.000	3.082	GIT	*i*	>20.92	–	This work
2024-11-11 03:05:18.000	3.480	SOAR/Goodman	*g*	>22.40	–	This work
2024-11-11 03:24:00.000	3.490	SOAR/Goodman	*r*	>22.90	–	This work
2024-11-11 03:38:26.000	3.510	SOAR/Goodman	*i*	>22.70	–	This work
2024-11-12 16:02:47.600	5.078	GIT	*r*	>20.86	–	This work
2024-11-12 16:29:24.200	5.097	GIT	*i*	>20.56	–	This work

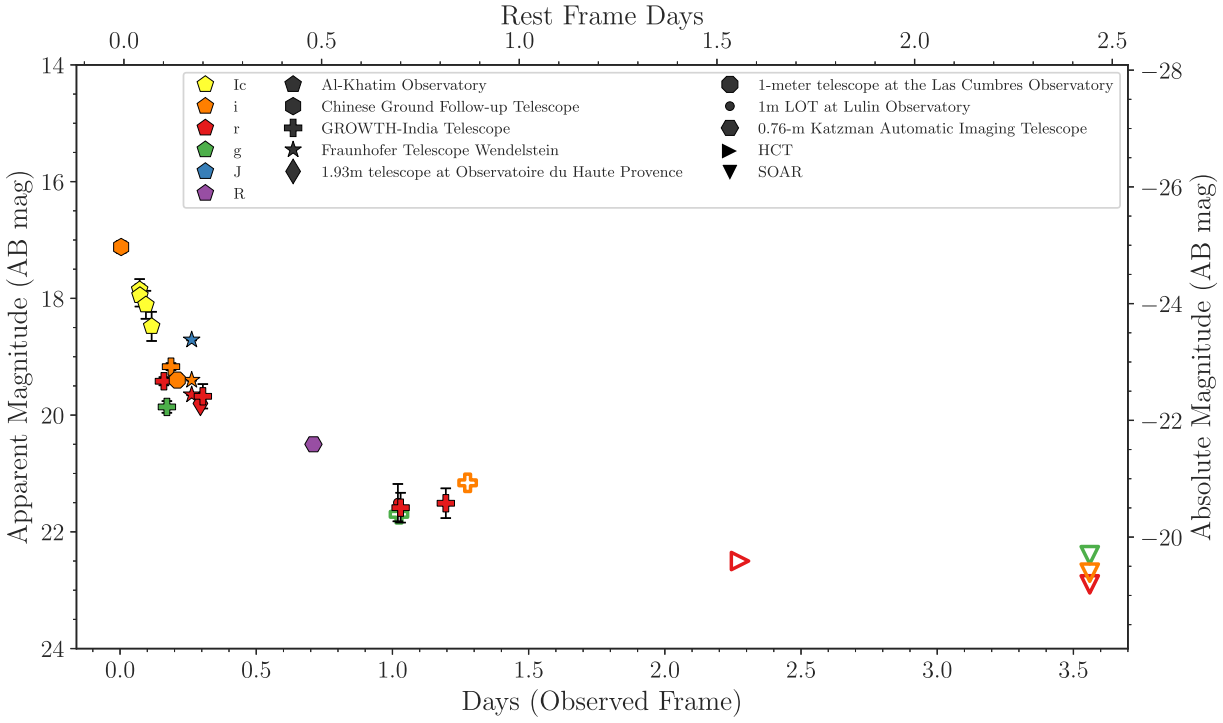

Figure 2. Optical photometry of the counterpart to EP241107a. We present the data obtained from our follow-up observations along with the data obtained from the GCNs. Different telescopes are denoted with different markers, while filters are indicated by various colours. The upper limits obtained from our observations are represented by open markers. We consider the T_0 to be the time of the EP-WXT trigger. Chinese Ground Follow-up Telescope at Changchun Observatory started the observation of the field of EP241107a about six minutes after the trigger and detected the counterpart in i filter at a magnitude of 17.12±0.10. The secondary x- and y-axes assume a redshift of $z = 0.457 \pm 0.003$.

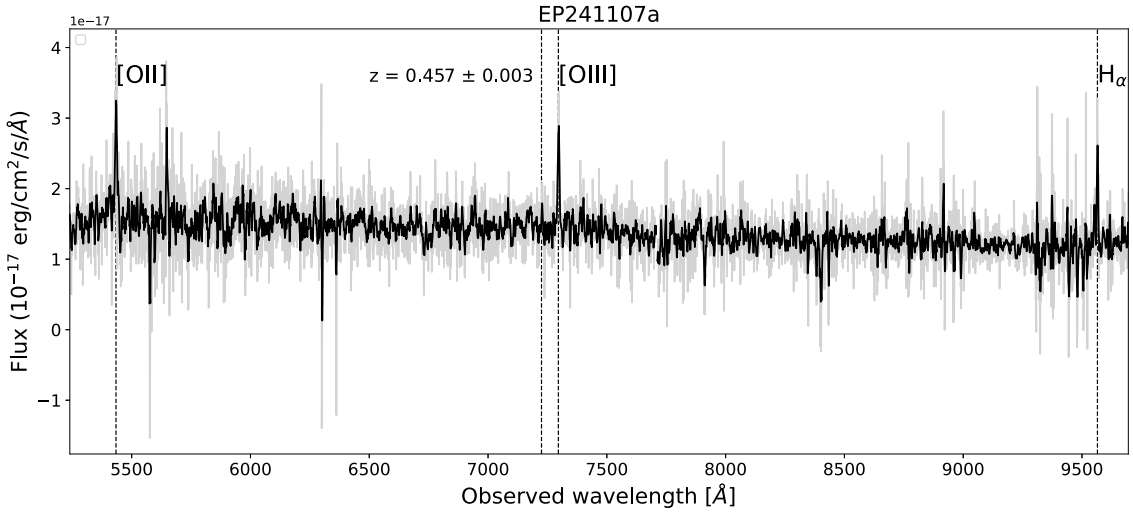

Figure 3. The flux-calibrated Keck LRIS spectrum of the counterpart of EP241107a taken 0.767 d after the EP-trigger is shown. For display purposes, the boxcar smoothed spectrum (Box1DKernel with a width of 5 pixels) is shown in the black solid line, whereas the light grey shows the spectrum. The location of important emission lines in the spectrum is marked with dashed lines. The emission lines are the host contributions, and we derive a redshift of 0.457±0.003 from the emission lines.

PYTHON. The AFTERGLOWPY code calculates GRB afterglow light curves and spectra (in Section 4, we discuss why we consider GRB as a viable model). It takes into consideration the effects of viewing angle and different jet structures. These structures describe how the energy of the jet changes with the jet opening angle θ_c.

The AFTERGLOWPY code allows the user to include viewing angle effects using the parameter $\theta_{\rm obs}$ and has an on-axis observation if $\theta_{\rm obs} = 0$. We assume a top-hat jet model for modelling the synchrotron emission from the jet interacting with the medium. For a uniform jet, the set of free parameters is $\Theta = \{E_0, \theta_c, \theta_{\rm obs}\ n_0,\ p,\ \epsilon_e,$ and

Table 2. Details of the jet afterglow model fitting. 100 walkers were initialized either evenly spaced within the respective bounds or clustered around the initial value.

Parameter	Bounds	Units	Prior	Posterior
$\log_{10}(E_0)$	(49, 54)	erg	logFlat	$51.16^{+0.07}_{-0.08}$
θ_c	$(0, \pi/6)$	deg	Flat	$0.26^{+0.03}_{-0.02}$
$\theta_{\rm obs}$	$(0, \pi/6)$	deg	Flat	$0.16^{+0.02}_{-0.03}$
p	(2, 3)	–	Flat	$2.202^{+0.036}_{-0.039}$
$\log_{10}(n_0)$	(−6,1)	$\rm cm^{-3}$	logFlat	$-1.19^{+0.15}_{-0.10}$
$\log_{10}(\epsilon_e)$	$(-4, \log_{10}(1/3))$	–	logFlat	$-0.70^{+0.10}_{-0.06}$
$\log_{10}(\epsilon_B)$	$(-8, \log_{10}(1/3))$	–	logFlat	> -0.97

$\epsilon_b\}$ where E_0, the isotropic-equivalent kinetic energy, θ_c is the half opening angle of the jet, n_0 is the density of the inter-stellar medium, p is the power-law index of the electron energy distribution, and ϵ_e and ϵ_b are the fraction of thermal energy that is imparted to electrons and magnetic fields, respectively. We fixed the fraction of shock-accelerated electrons $\xi_N = 1$ for our code. We fixed the luminosity distance d_L based on our spectroscopic redshift (see Section 2.4) and the adopted cosmological model mentioned in Introduction.

A SCIPY (P. Virtanen et al. 2020) OPTIMIZE routine was used to obtain better guess parameters for the Markov chain Monte Carlo (MCMC) walkers. 100 walkers were initialized around this guess parameter set and allowed to explore the parameter space, in order to maximize the likelihood. Some walkers got stuck in low-probability regions and did not allow the MCMC chains to converge. So, all walkers were re-initialized near the high probability region, allowing the MCMC chains to converge. The posterior values and corner plots to visualize the MCMC fit were computed using CHAINCONSUMER (S. R. Hinton 2016). The priors for our seven free parameters, the nature of the prior, and the posterior values obtained are given in the Table 2.

3.2 Modelling of the host of EP241107a using BAGPIPES

We determine the host properties of EP241107a using BAGPIPES (Bayesian Analysis of Galaxies for Physical Inference and Parameter Estimation; A. C. Carnall et al. 2018), incorporating the host magnitudes. Employing the MULTINEST sampling algorithm, BAGPIPES fits stellar population models to multiband photometric data, accounting for the star formation history and the transmission function of neutral and ionized interstellar medium (ISM) in broad-band photometry and spectra.

The posterior probability distributions for the host galaxy age, dust extinction (A_V), star formation rate (SFR), metallicity (Z), stellar mass (M_*), and specific SFR (sSFR) are obtained through fitting with BAGPIPES, assuming a flat prior for the redshift based on the spectroscopic redshift. We adopt an exponentially declining star formation history function and apply the dust attenuation parametrization developed by D. Calzetti et al. (2000) to model the spectral energy distributions (SEDs), using priors for A_V in the range of 0.0 to 2.0 mag. The input observed photometric data are shown in blue. The 16th–84th percentile range of the posterior probability distribution for the spectrum and broad-band photometry (shaded in light orange and orange) is presented in Fig. 4. We utilized the publicly available photometric magnitudes of the candidate host galaxy of EP241107a from the Dark Energy Spectroscopic Instrument (DESI) Legacy Imaging Survey Archive (A. Dey et al. 2019). The reported magnitudes are $g = 23.64 \pm 0.08$,

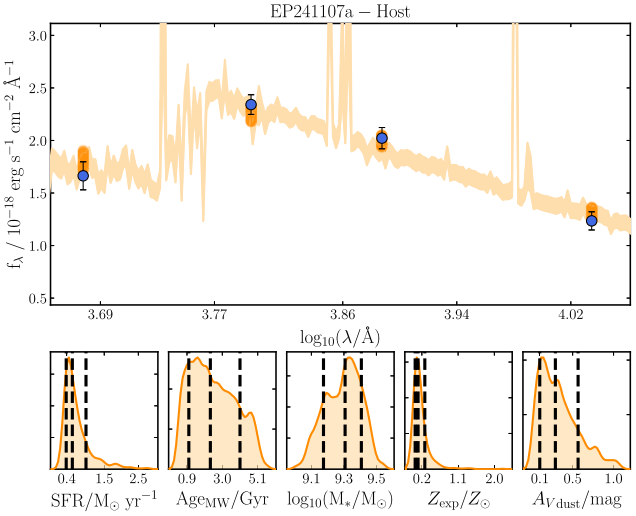

Figure 4. The best-fitting SED model of the host of EP241107a using BAGPIPES package is shown. The blue markers give the photometric data, and their 1σ uncertainties, whereas the 16th–84th percentile range for the posterior probability for the spectrum and photometry are shown in light and dark orange colours, respectively. The bottom panel shows the posterior probability distributions for the five fitted parameters, SFR, age, galaxy stellar mass, metallicity, and dust extinction. In each subplot, the 16th, 50th, and 84th percentile posterior values are represented by vertical dashed black lines marked from left to right.

$r = 22.68 \pm 0.04$, $i = 22.39 \pm 0.05$, and $z = 22.19 \pm 0.07$. The inferred host properties are discussed in Section 4.4.

4 DISCUSSION

4.1 FXT properties and energetics

We begin with the discussion on the X-ray observations of EP241107a. EP241107a showed a peak flux of approximately 4.2×10^{-9}erg cm^{-2} s^{-1} in the 0.5–4 keV band (R. Z. Li et al. 2024). Given its spectroscopic redshift of ~ 0.457, the inferred X-ray luminosity at trigger is $\sim 3.4 \times 10^{48}$ erg s^{-1} (in the 0.5–4 keV band by EP-WXT). This luminosity is higher compared to the predicted X-ray luminosities of typical SN SBOs ($L_{\rm X,peak} \lesssim 10^{45}$ erg s^{-1} for supernova SBOs; A. M. Soderberg et al. 2008; E. Waxman & B. Katz 2017; J. A. Goldberg et al. 2022). Approximately 60 min post-trigger, an X-ray afterglow with a luminosity of 1.2×10^{46} erg s^{-1} was detected by EP-FoXT in the 0.5–10 keV band. This X-ray counterpart declined rapidly and went undetected ∼3.9 d post-trigger in the same energy band (R. Z. Li et al. 2024). No γ-ray association has been reported so far for EP241107a,[7] through General Coordinates Network (GCN) circulars . Y.-Q. Zhang et al. (2025) report the absence of gamma detection for EP241107a from multi-instrument search.

4.2 Optical evolution: comparison with known transient classes

In Fig. 5, we compare the optical light curve of EP241107a, corrected for Galactic extinction,[8] with the light curves of SNe, GRB

[7] At the time of writing.
[8] Calculated using https://ned.ipac.caltech.edu/extinction_calculator $A_V = 0.3$, and $R_V \sim 3.1$.

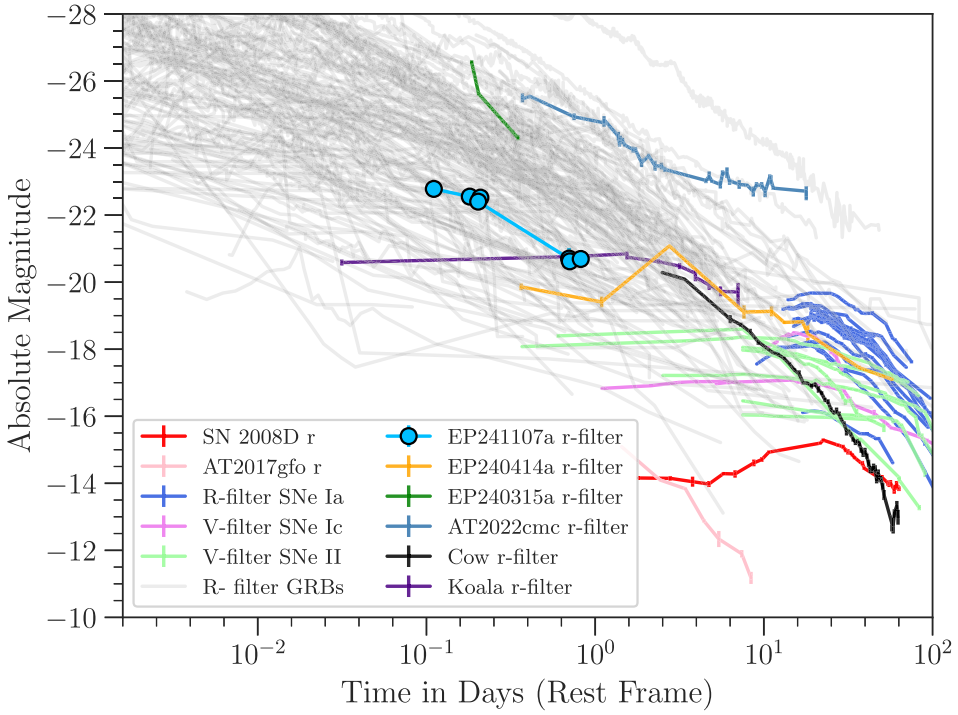

Figure 5. The optical light curve of EP241107a (*r* filter; shown in skyblue) in comparison with the light curves of SN2008D (A. M. Soderberg et al. 2008), AT2017gfo (P. S. Cowperthwaite et al. 2017), Type II SNe, Type Ia SNe, Type Ic SNe (K. Iwamoto et al. 2000; S. Jha et al. 2006; M. Modjaz et al. 2006; M. Hicken et al. 2017), GRB afterglows (D. A. Kann et al. 2010; D. A. Kann et al. 2011), the optical counterpart of EP240315a (A. J. Levan et al. 2024; J. H. Gillanders et al. 2024), EP240414a (J. N. D. Dalen et al. 2025; S. Srivastav et al. 2025), AT2018cow (the 'Cow'; D. A. Perley et al. 2019), ZTF18abvkwla (the 'Koala'; A. Y. Q. Ho et al. 2020), and the jetted TDE AT2022cmc (I. Andreoni et al. 2022). The magnitudes are corrected for the Galactic extinction. The light curve of EP241107a is consistent with the GRB afterglow light curves.

afterglows, other EP FXTs, and FBOTs. We infer that the light curve EP241107a is consistent with the population of GRB afterglows[9] (shown in grey in Fig. 5). The *r*-filter light curves of EP240315a and EP240414a (J. N. D. Dalen et al. 2025; J. H. Gillanders et al. 2024; A. J. Levan et al. 2024; S. Srivastav et al. 2025) also fall within the parameter space occupied by the GRB population similar to EP241107a. That said, EP240414a was found to be associated with the core-collapse of a massive star, resulting in a broad-line Type Ic SNe seen in lGRBs and its evolution does not resemble the light curve of EP241107a. Furthermore, the association of EP241107a with AT2018cow-like transients appears unlikely based on a comparison of their optical light curves.

We observe a two-phase temporal evolution in the *r*-filter light curve of EP241107a, with decay indices for the initial phase (prior to 0.3 d) to be $\alpha = 0.46 \pm 0.12$ and a later phase with an $\alpha = 1.33 \pm 0.13$. These decay indices are consistent with the optical afterglow light curves of GRBs (D. A. Kann et al. 2010). The rapid optical decay is not consistent with the slow evolution typical of TDE light curves in the early phase (S. Velzen et al. 2020). Based on these optical light curve comparisons, we conclude that EP241107a is most likely associated with the GRB afterglow population, representing a new addition to the growing catalogue of EP-discovered GRBs.

4.3 Insights from the radio observations

In Fig. 6, we show 3σ radio upper limits from our uGMRT observations and detections from VLA observations at 6 and 10 GHz. These limits and detections are compared with the radio light curves of other extragalactic transients in radio. The specific luminosity has been *K*-corrected (D. W. Hogg et al. 2002) to account for the cosmological distances of some sources. Additionally, we compare our upper limits with the radio light curves of previously reported EP-FXTs, namely EP240315a (J. H. Gillanders et al. 2024; R. Ricci et al. 2025), EP240414a (J. S. Bright et al. 2025), and the radio upper limits for the FXT XRT210423 (D. Eappachen et al. 2023), discovered from the *Chandra* archival data (D. Ibrahimzade et al. 2025). We infer that the VLA detections in both bands (see the star marker in Fig. 6) are in agreement with the parameter space occupied by the radio afterglows of GRBs. We note that it is likely that the non-detection in the lower frequencies for EP241107a might be because of absorption processes (R. A. Chevalier 1998). In summary, the radio detection for EP241107a strongly supports a GRB-like afterglow.

4.4 Comparison of host properties

We found a faint associated host centred at RA $= 02^{h}20^{m}02.40^{s}$, Dec. $= +03^{\circ}\ 20'\ 02.33''$ which is ~ 0.83 arcsec from the counterpart reported by M. Odeh et al. (2024a) in the DESI legacy images for EP241107a. At the redshift of $\sim$0.457, the projected offset is 4.8 kpc. This galactocentric offset places EP241107a at the $\sim$90th percentile of lGRB offset distribution (J. D. Lyman et al. 2017), while it is also in agreement with the $\sim$40 percentile of sGRB offsets (W.-f. Fong et al. 2022; B. O'Connor et al. 2022).

Using BAGPIPES and observed magnitudes of the candidate host in *g*, *r*, *i*, and *z* filters from the legacy archive, we estimated

[9]For comparison, we consider the *R* and *r* filters to be similar.

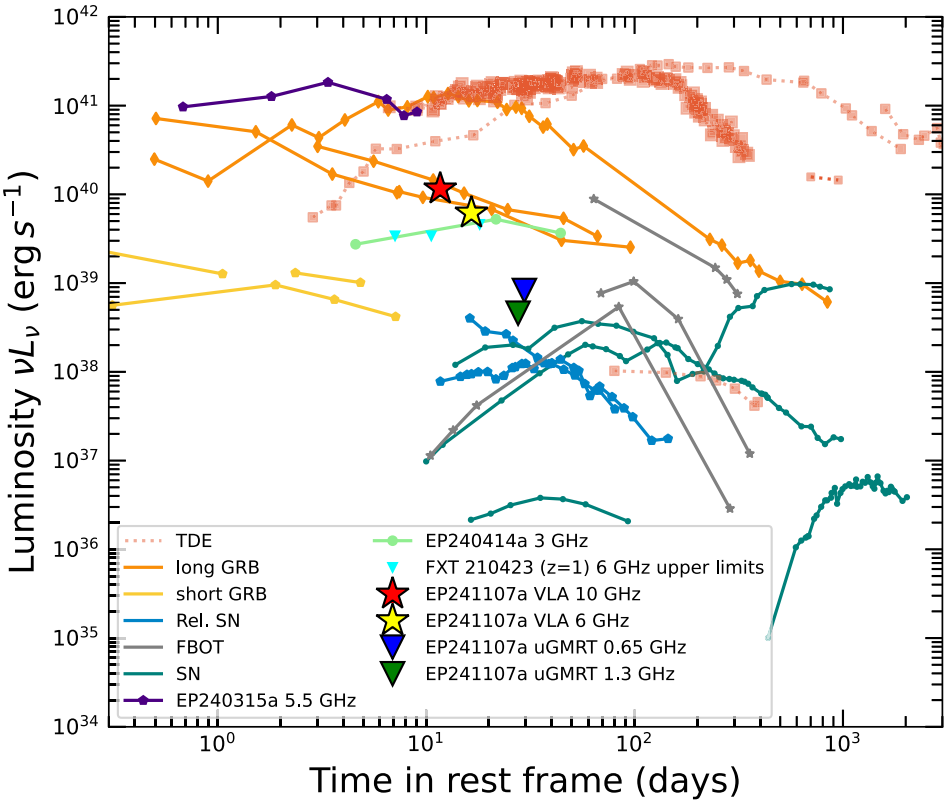

Figure 6. The uGMRT and VLA radio observations of EP241107a compared with other extragalactic transients in radio, including relativistic supernovae, LFBOTs (D. L. Coppejans et al. 2020), thermal TDEs (K. D. Alexander et al. 2020), relativistic TDEs (T. Eftekhari et al. 2018; L. Rhodes et al. 2023), short GRBs (W. Fong et al. 2021), long GRBs (E. Berger et al. 2003; A. J. der Horst et al. 2014; T. Laskar et al. 2023), and LL-GRBs (S. R. Kulkarni et al. 1998; A. M. Soderberg et al. 2010). The specific luminosity has been *K*-corrected to account for the cosmological distances of some sources. This plot is based on fig. 9 in A. Y. Q. Ho et al. (2020), and references therein.

the host properties for EP241107a. A SFR of $0.6^{+0.4}_{-0.2}$ $M_\odot yr^{-1}$ and $\log(M_*[M_\odot])$ of 9.3 ± 0.1 is estimated for the candidate host of EP241107a. Fig. 7 shows the M_* and SFR of the host galaxy of EP241107a (gold star) compared with host galaxies of the previously reported FXTs (F. E. Bauer et al. 2017; J. Quirola-Vásquez et al. 2022; D. Eappachen et al. 2023, D. Eappachen et al. 2024; J. N. D. Dalen et al. 2025; J. Quirola-Vásquez et al. 2025), of lGRBs, sGRBs, low-luminosity lGRBs (K. Wiersema et al. 2007; L. Christensen et al. 2008; M. J. Michałowski et al. 2014; E. M. Levesque 2014; Y. Li, B. Zhang & H.-J. Lü 2016; T. Krühler et al. 2017; J. Wang et al. 2018; M. Arabsalmani et al. 2019; W.-f. Fong et al. 2022), and SN Ic (S. Schulze et al. 2021). Though the M_* and SFR of the host galaxy of EP241107a are consistent with the populations of hosts of lGRBs and sGRBs, it takes up the parameter space previously not occupied by the *Chandra–XMM–Newton* FXTs.

It is worth noting that the host properties inferred for EP241107a are based only on four observed magnitudes. Although our SED modelling provides an estimate of the host properties, deeper observations of the host galaxies would significantly improve our understanding of their environments and will be crucial in constraining the nature of the transients. A pertinent example is the case of CDF-XT2, where deeper *James Webb Space Telescope* observations of the host galaxy by J. Quirola-Vásquez et al. (2025) improved upon the earlier host properties reported by Y. Q. Xue et al. (2019), thereby better constraining the nature of the transient.

4.5 Constraints on relativistic jets

For EP241107a, we discuss the jet parameters that we infer from our AFTERGLOWPY modelling discussed in Section 3.1. We consider the simple uniform jet, which is sufficient to provide a good fit of the data set. The broad-band AFTERGLOWPY light curves from radio to the X-ray band of EP241107a are shown in Fig. 8. Note that the light curves are scaled for visual purposes. The corner plot of the posterior fit parameters is given in Fig. A1. Our fit yields a jet of $E_{\rm K,iso} \sim 10^{51}$ erg with a $\theta_c \approx 15^\circ$ viewed at an angle of $\theta_{\rm obs} \approx 9^\circ$ which agrees with the population of cosmological GRBs. The best fit $n_0 \approx 10^{-1.2}$ cm^{-3}, suggesting a typical low-density ISM environment for EP241107a (P. Chandra & D. A. Frail 2012). The value of the power-law index of the electron energy distribution p from the best-fitting model ∼2.2, agrees with the value (p =2.3; U. Keshet & E. Waxman 2005) inferred from the shock acceleration principle. We infer that in the case of 1.3 GHz observation, our upper limits do not agree with the best-fitting light curve. One explanation could be that AFTERGLOWPY does not account for synchrotron self-absorption. The radio data show evidence for a jet break (for the 6 GHz light curve, we see a jet break around 10 d since the trigger).

Although our model favours an on-axis scenario ($\theta_{\rm obs} < \theta_c$), no gamma-ray detections were reported for EP241107a.[10] Considering

[10]At the time of writing.

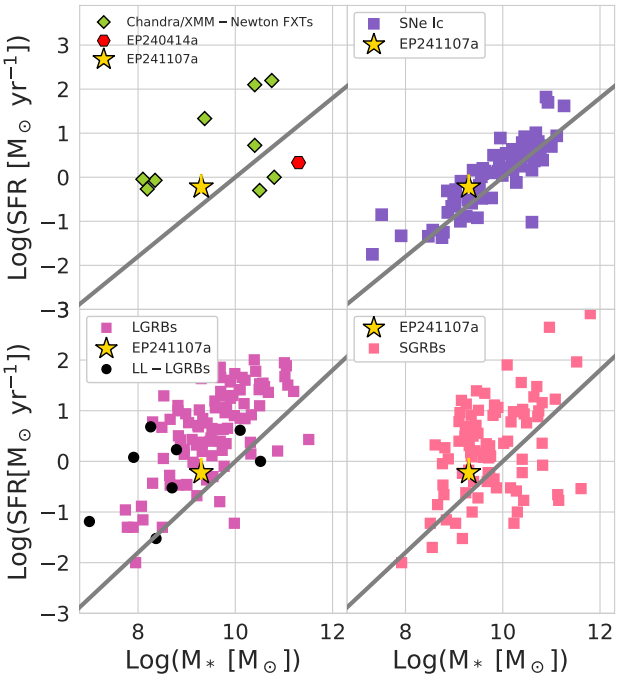

Figure 7. M_* and SFR of the host galaxy of EP241107a (yellow star) compared with host galaxies of other transient events. Different panels show the host properties of the previously reported FXTs (F. E. Bauer et al. 2017; Y. Q. Xue et al. 2019; J. Quirola-Vásquez et al. 2022; D. Eappachen et al. 2023, 2024; J. N. D. Dalen et al. 2025), of lGRBs, sGRBs, low-luminosity lGRBs (K. Wiersema et al. 2007; L. Christensen et al. 2008; M. J. Michałowski et al. 2014; E. M. Levesque 2014; Y. Li et al. 2016; T. Krühler et al. 2017; J. Wang et al. 2018; M. Arabsalmani et al. 2019; W.-f. Fong et al. 2022), and SN Ic (S. Schulze et al. 2021). The solid grey lines show the best-fitting local galaxy main sequence relation from Y.-j. Peng et al. (2010).

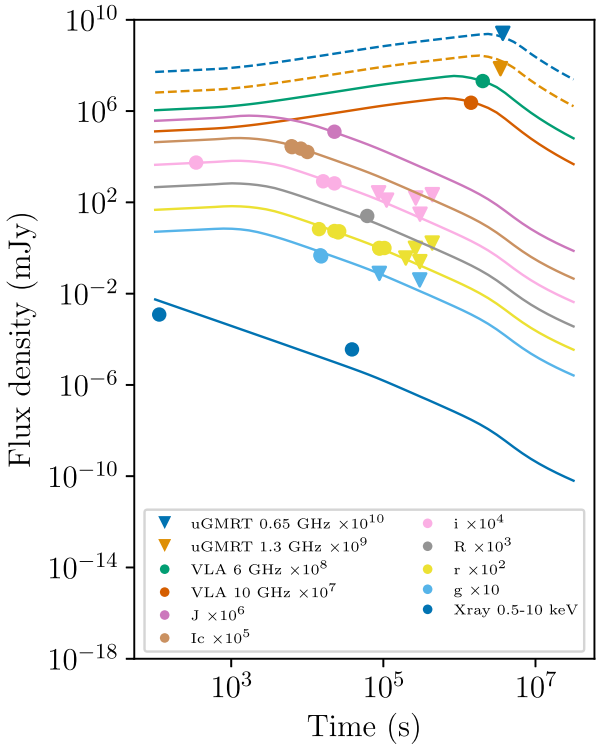

Figure 8. The broad-band AFTERGLOWPY modelling of EP241107a is presented, where the figure shows the best-fitting light curves. Each data point represents observed flux density in different bands ranging from X-ray to radio. Upper limits are indicated by inverted triangles. Note that the light curves are scaled for visual purposes. The best-fitting jet parameters inferred from the AFTERGLOWPY modelling are discussed in detail in Section 4.5.

the best fit $E_{\rm K,iso} \sim 1.4 \times 10^{51}$ erg and the $\theta_c \approx 15^\circ$, the beaming corrected kinetic energy $E_K = (1 - \text{-cos } \theta_c)\ E_{\rm K,iso} \approx 4.8 \times 10^{49}$ erg. This beam corrected kinetic energy of 4.8 $\times 10^{49}$ erg, is at the lower end of the distribution of classical GRBs (X.-G. Wang et al. 2018). Hence, the lack of gamma-rays could be interpreted as EP241107a being an intrinsically low-energy GRB. Though the energy scales match with a few relativistic TDEs (e.g. XMMSL1 J0740−85; K. D. Alexander et al. 2016; R. D. Saxton et al. 2017), we would expect the density of the medium to be three orders of magnitude greater in the case of TDEs (F. De Colle & W. Lu 2020). The optical counterpart of EP241107a is roughly 10 times fainter than the typical GRB afterglows one day after the trigger, when compared to the golden sample of D. A. Kann et al. (2010). Therefore, while EP241107a exhibits the energetics and jet geometry typical of cosmological GRBs, the absence of gamma-ray emission despite its inferred on-axis viewing geometry suggests that this event represents an intrinsically faint GRB at the lower end of the classical GRB energy distribution.

4.6 Evaluating EP241107a in the landscape of FXTs

In this section, we examine the nature of EP241107a in relation to the broader FXT population detected by *EP*, *Chandra*, *XMM–Newton*, and *Swift*. In Fig. 9, the peak X-ray luminosity of EP241107a (yellow) is compared with those of extragalactic FXTs observed by *Chandra*

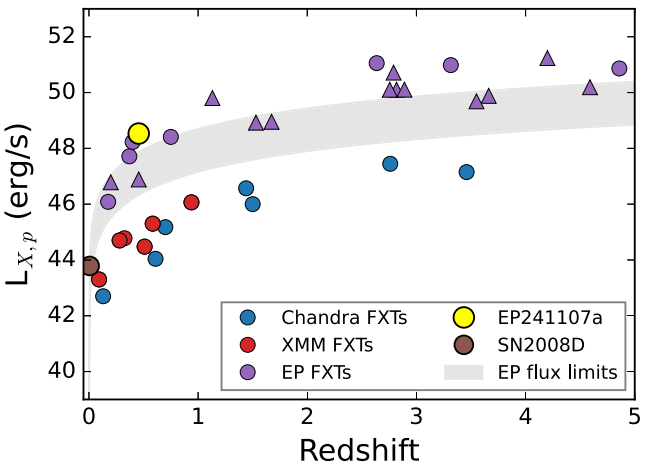

Figure 9. The peak X-ray luminosity of EP241107a (yellow marker) is compared with those of extragalactic FXTs observed by *Chandra* (J. Quirola-Vásquez et al. 2022; J. Quirola-Vásquez et al. 2023), *XMM–Newton* (D. Alp & J. Larsson 2020; D. Eappachen et al. 2024; A. Inkenhaag et al. 2024), and EP (from GCNs reported by the EP team; W. Yuan et al. 2022) as a function of redshift. The upward triangle shows the limit on the peak X-ray luminosity (often, in the case of EP-FXTs, the EP team reports the average unabsorbed flux). We also plot the sensitivity curve for EP (W. Yuan et al. 2022). The details of pre-EP era FXTs are given in Table A1.

(J. Quirola-Vásquez et al. 2022; D. Lin et al. 2022; J. Quirola-Vásquez et al. 2023; D. Eappachen et al. 2023; D. Ibrahimzade et al. 2025), *XMM–Newton* (D. Alp & J. Larsson 2020; D. Eappachen et al. 2024; A. Inkenhaag et al. 2024), *Swift* (A. M. Soderberg et al. 2008), and EP (from GCNs reported by EP team; W. Yuan et al. 2022) as a function of redshift (similar to the figure from S. Srivastav et al. 2025). The limit on the peak X-ray luminosity (often in the case of EP-FXTs, the EP team reports the average unabsorbed flux) is shown with an upward triangle. The sensitivity curve for EP is also plotted in the Fig. 9.

The extragalactic FXTs discovered from *Chandra* and *XMM–Newton* show peak X-ray luminosities ranging from $L_{X,p} \sim 10^{42}$–10^{47} erg s^{-1}, at redshifts $z \sim 0.09$–3.5. The most distant FXT among the pre-EP era is CDF-XT2, which is at a redshift of ∼3.5 with a peak X-ray luminosity of $\approx 10^{47}$ erg s^{-1}(J. Quirola-Vásquez et al. 2025).

On the other hand, EP-discovered FXTs exhibit peak X-ray luminosities of $L_{X,p} > 10^{46}$ erg s^{-1} and span a redshift range of $z \sim$ 0.176–4.859, with a mean redshift of $z \sim 2$. The nearest EP-detected FXT with a spectroscopic redshift is EP250108a at $z = 0.176$ (R. A. J. Eyles-Ferris et al. 2025; W. X. Li et al. 2025; G. P. Srinivasaragavan et al. 2025; J. C. Rastinejad et al. 2025), which was associated with the closest known broad-lined Type Ic SN discovered by EP; meanwhile, the most distant case is of EP240315a (J. H. Gillanders et al. 2024; A. J. Levan et al. 2024; Y. Liu et al. 2025).

FXTs exhibit diverse properties and are believed to originate from a variety of progenitor mechanisms. For example, CDF–XT2, discovered in the *Chandra* archive, may be associated with a low-luminosity collapsar progenitor (Y. Q. Xue et al. 2019; J. Quirola-Vásquez et al. 2025), while FXT XRT 110621, found through a search of archival *XMM–Newton* data, could plausibly be an SN SBO (D. Alp & J. Larsson 2020; D. Eappachen et al. 2024). Additionally, FXTs such as XRT 210 423 (D. Eappachen et al. 2022; D. Ibrahimzade et al. 2025) may be linked to a BNS merger scenario, in which the central engine is powered by a millisecond magnetar (B. D. Metzger & A. L. Piro 2014; H. Sun et al. 2017; C. Chen, Y. Wang & B. Zhang 2025). However, S. Biswas et al. (2025) considered all plausible formation pathways for millisecond magnetars that could produce an FXT and inferred that such progenitors can account for at most 10 per cent of the entire FXT population. Also, a TDE origin remains a plausible explanation for FXTs like XRT 000519 (P. G. Jonker et al. 2013; D. Eappachen et al. 2022). As seen in the Fig. 9, the variety of FXT progenitor scenarios is reflected in the wide range of X-ray luminosities and associated redshifts. S. Srivastav et al. (2025) point out that the X-ray luminosity parameter space explored by EP is distinct from that of previously discovered FXTs by *Chandra* and *XMM–Newton*, owing to the different observing strategy, probing high redshift and intrinsically more luminous events.

A large number of EP-discovered FXTs have been associated with GRBs or show similar properties to them (for e.g. A. J. Levan et al. 2024). EP241107a properties also agree with the typical afterglow nature seen in GRBs. EP241107a is consistent with the population of FXTs detected by EP and are mostly distinct from the population of FXTs detected by *Chandra* and *XMM–Newton*. CDF-XT1 and CDF-XT2 are exceptions as they are associated with host galaxies at z>2.5. However, at least for some of the *Chandra* and *XMM–Newton* FXTs, the energetics might vary with future deeper observations of the host, as some might be wrongly associated with the host at a different redshift (for e.g. see J. Quirola-Vásquez et al. 2025).

5 CONCLUSION

We present the multiwavelength follow-up of an EP-detected FXT EP241107a. A radio counterpart was detected at 10 and 6 GHz with flux densities of 232 ± 9 and 207 ± 8 μJy, respectively, between ∼16–24 d after the X-ray trigger. We compared the radio and optical light curves of EP241107a with those of other transients and found that EP241107a is consistent with the parameter space occupied by GRB afterglows.

We also examined the host properties of EP241107a and the host offsets, SFR and M_*, which match with the population of GRBs. We modelled the multiwavelength afterglow for EP241107a and inferred the jet properties. Our fit yields a jet of $E_{\rm K,iso} \sim 10^{51}$ erg with a $\theta_c \approx 15^\circ$ viewed at an angle of $\theta_{\rm obs} \approx 9^\circ$. The absence of gamma-ray emission, the inferred on-axis viewing geometry and the energetics derived from afterglow modelling suggest that EP241107a is an intrinsically faint GRB.

Finally, we compared the population of EP-FXTs with those detected by the *Chandra*, *XMM–Newton*, and *Swift* detected FXTs from the pre-EP era. EP241107a is consistent with the population of FXTs detected by EP and are mostly distinct from the population of FXTs detected by *Chandra* and *XMM–Newton*. However, at least for some of the pre-EP era FXTs, the energetics may change with future deeper observations of the host, as some might be wrongly associated with a host at a different redshift. The *EP* mission is detecting a significant number of FXTs, which may be associated with diverse progenitor mechanisms, highlighting the importance of prompt and multiwavelength follow-up observations to characterize and better understand the nature of these EP-FXTs.

ACKNOWLEDGEMENTS

We thank the anonymous referee for the helpful comments. DE thank Jonathan Quirola-Vásquez, Ashley Chrimes, Judhajeet Basu, and Hrishav Das for the useful discussions. DE acknowledges Lauren Rhodes for sharing the radio data of transients. AB and DE also thank Suvedha Suresh Naik for the discussions on MCMC. DE acknowledges the use of AI language models (Claude by Anthropic and ChatGPT by OpenAI) for assistance with code editing, data visualization, spell checking, and grammar correction. GCA acknowledges support from the Indian National Science Academy (INSA) through its Senior Scientist Programme.

We thank the staff of the uGMRT that made these observations possible. uGMRT is run by the National Centre for Radio Astrophysics of the Tata Institute of Fundamental Research. The uGMRT observations of EP241107a were carried out under ddtC404, with D. Eappachen as PI.

The National Radio Astronomy Observatory is a facility of the National Science Foundation operated under cooperative agreement by Associated Universities, Inc. Our EP241107a Very Large Array (VLA) observations were carried out under the DDT proposal 24B-492 (PI: Balasubramanian).

This work is partially based on data obtained with the 2-m Himalayan Chandra Telescope of the Indian Astronomical Observatory (IAO) under the proposal HCT-2024-C3-P32 (PI: D. Eappachen). We thank the staff of IAO, Hanle, and CREST, Hosakote, that made these observations possible. The facilities at IAO and CREST are operated by the Indian Institute of Astrophysics, Bangalore.

The GROWTH India Telescope (GIT) is a 70-cm telescope with a 0.7° field of view, set up by the Indian Institute of Astrophysics (IIA) and the Indian Institute of Technology Bombay (IITB) with funding from Indo-US Science and Technology Forum and the

Science and Engineering Research Board, Department of Science and Technology, Government of India. It is located at the IAO (Hanle), operated by IIA. We acknowledge funding by the IITB alumni batch of 1994, which partially supports the operations of the telescope.

Some of the data presented herein were obtained at Keck Observatory, which is a private 501(c)3 non-profit organization operated as a scientific partnership among the California Institute of Technology, the University of California, and the National Aeronautics and Space Administration. The Observatory was made possible by the generous financial support of the W. M. Keck Foundation. The authors wish to recognize and acknowledge the very significant cultural role and reverence that the summit of Maunakea has always had within the Native Hawaiian community. We are most fortunate to have the opportunity to conduct observations from this mountain.

Based on observations obtained at the Southern Astrophysical Research (SOAR) telescope, which is a joint project of the Ministério da Ciência, Tecnologia e Inovações (MCTI/LNA) do Brasil, the US National Science Foundation's NOIRLab, the University of North Carolina at Chapel Hill (UNC), and Michigan State University (MSU).

DATA AVAILABILITY

The data relevant to this article will be shared on request to the corresponding author.

REFERENCES

Adami C., Dennefeld M., Coleiro A., Basa S., Le Floc'h E., 2024, GCN Circ., 38122, 1
Alexander K. D., Berger E., Guillochon J., Zauderer B. A., Williams P. K. G., 2016, ApJ, 819, L25
Alexander K. D., van Velzen S., Horesh A., Zauderer B. A., 2020, Space Sci. Rev., 216, 81
Alp D., Larsson J., 2020, ApJ, 896, 39
Andreoni I. et al., 2022, Nature, 612, 430
Arabsalmani M. et al., 2019, MNRAS, 485, 5411
Bauer F. E. et al., 2017, MNRAS, 467, 4841
Berger E. et al., 2003, Nature, 426, 154
Biswas S., Jonker P. G., Miller M. C., Levan A., Quirola-Vásquez J., 2025, A&A, 700, A161
Bright J. S. et al., 2025, ApJ, 981, 48
Busmann M. et al., 2025, A&A, 701, A225
Busmann M., Gruen D., O'Connor B., 2024, GCN Circ., 38120, 1
Calzetti D., Armus L., Bohlin R. C., Kinney A. L., Koornneef J., Storchi-Bergmann T., 2000, ApJ, 533, 682
Carnall A. C., McLure R. J., Dunlop J. S., Davé R., 2018, MNRAS, 480, 4379
CASA Team et al., 2022, PASP, 134, 114501
Chambers K. C. et al., 2016, preprint (arXiv:1612.05560)
Chandra P., Frail D. A., 2012, ApJ, 746, 156
Chen C., Wang Y., Zhang B., 2025, preprint (arXiv:2505.01606)
Chevalier R. A., 1998, ApJ, 499, 810
Christensen L., Vreeswijk P. M., Sollerman J., Thöne C. C., Le Floc'h E., Wiersema K., 2008, A&A, 490, 45
Clemens J. C., Crain J. A., Anderson R., 2004, in Moorwood A. F. M., Iye M., eds, Proc. SPIE Conf. Ser. Vol. 5492, Ground-based Instrumentation for Astronomy. SPIE, Glasgow, UK, p. 331
Coppejans D. L. et al., 2020, ApJ, 895, L23
Cowperthwaite P. S. et al., 2017, ApJ, 848, L17
De Colle F., Lu W., 2020, New Astron. Rev., 89, 101538
Dey A. et al., 2019, AJ, 157, 168
Eappachen D. et al., 2022, MNRAS, 514, 302
Eappachen D. et al., 2023, ApJ, 948, 91
Eappachen D. et al., 2024, MNRAS, 527, 11823
Eftekhari T., Berger E., Zauderer B. A., Margutti R., Alexander K. D., 2018, ApJ, 854, 86
Eyles-Ferris R. A. J. et al., 2025, ApJ, 988, L14
Fong W. et al., 2021, ApJ, 906, 127
Fong W.-f. et al., 2022, ApJ, 940, 56
Foreman-Mackey D., Hogg D. W., Lang D., Goodman J., 2013, PASP, 125, 306
Freeburn J., Andreoni I., Carney J., 2024, GCN Circ., 38208, 1
Gianfagna G. et al., 2025, A&A, 703, A92
Gillanders J. H. et al., 2024, ApJ, 969, L14
Glennie A., Jonker P. G., Fender R. P., Nagayama T., Pretorius M. L., 2015, MNRAS, 450, 3765
Goldberg J. A., Jiang Y.-F., Bildsten L., 2022, ApJ, 933, 164
Hicken M. et al., 2017, ApJS, 233, 6
Hinton S. R., 2016, J. Open Source Softw., 1, 00045
Ho A. Y. Q. et al., 2020, ApJ, 895, 49
Hogg D. W., Baldry I. K., Blanton M. R., Eisenstein D. J., 2002, preprint (arXiv:astro-ph/0210394)
Hu L., Wang L., Chen X., Yang J., 2022, ApJ, 936, 157
Ibrahimzade D. et al., 2025, ApJ, 980, 92
Inkenhaag A., Jonker P. G., Levan A. J., Quirola-Vásquez J., Bauer F. E., Eappachen D., 2024, A&A, 689, A343
Iwamoto K. et al., 2000, ApJ, 534, 660
Jha S. et al., 2006, AJ, 131, 527
Jonker P. G. et al., 2013, ApJ, 779, 14
Jonker P. G. et al., 2025, MNRAS, preprint (arXiv:2508.13039)
Kale R., Ishwara-Chandra C. H., 2021, Exp. Astron., 51, 95
Kang Z., Wu C., Xin L., 2024, GCN Circ., 38116, 1
Kann D. A. et al., 2010, ApJ, 720, 1513
Kann D. A. et al., 2011, ApJ, 734, 96
Keshet U., Waxman E., 2005, Phys. Rev. Lett., 94, 111102
Kong A. K. H. et al., 2024, GCN Circ., 38131, 1
Krühler T., Kuncarayakti H., Schady P., Anderson J. P., Galbany L., Gensior J., 2017, A&A, 602, A85
Kulkarni S. R. et al., 1998, Nature, 395, 663
Kumar H. et al., 2022, AJ, 164, 90
Lang D., Hogg D. W., Mierle K., Blanton M., Roweis S., 2010, AJ, 139, 1782
Laskar T. et al., 2023, ApJ, 946, L23
Levan A. J. et al., 2024, preprint (arXiv:2404.16350)
Levan A. J. et al., 2025, preprint (arXiv:2507.14286)
Levesque E. M., 2014, PASP, 126, 1
Li R. Z., Chen W., Chatterjee K., Chen X. L., Zhou H., Zhao T., Pan H. W., Einstein Probe Team, 2024, GCN Circ., 38171, 1
Li W. X. et al., 2024, GCN Circ., 38127, 1
Li W. X. et al., 2025, preprint (arXiv:2504.17034)
Li Y., Zhang B., Lü H.-J., 2016, ApJS, 227, 7
Lin D., Irwin J. A., Berger E., Nguyen R., 2022, ApJ, 927, 211
Liu Y. et al., 2025, Nat. Astron., 9, 564
Lyman J. D. et al., 2017, MNRAS, 467, 1795
MacLeod M., Guillochon J., Ramirez-Ruiz E., Kasen D., Rosswog S., 2016, ApJ, 819, 3
Maguire K., Eracleous M., Jonker P. G., MacLeod M., Rosswog S., 2020, Space Sci. Rev., 216, 39
Metzger B. D., Piro A. L., 2014, MNRAS, 439, 3916
Michałowski M. J. et al., 2014, A&A, 562, A70
Modjaz M. et al., 2006, ApJ, 645, L21
Nakar E., Piran T., 2017, ApJ, 834, 28
Novara G. et al., 2020, ApJ, 898, 37
O'Connor B. et al., 2022, MNRAS, 515, 4890
O'Connor B. et al., 2025a, ApJ, 993, L37
O'Connor B. et al., 2025b, ApJ, 979, L30
Odeh M., Alshamsi S., Pattani N. M., Guessoum N., 2024a, GCN Circ., 38115, 1
Odeh M., Alshamsi S., Pattani N. M., 2024b, GCN Circ., 38128, 1
Oke J. B. et al., 1995, PASP, 107, 375
Pastor-Marazuela I., Webb N. A., Wojtowicz D. T., van Leeuwen J., 2020, A&A, 640, A124
Peng Y.-j. et al., 2010, ApJ, 721, 193

Perley D. A. et al., 2019, MNRAS, 484, 1031
Perley D. A., 2019, PASP, 131, 084503
Planck Collaboration XIII, 2016, A&A, 594, A13
Prentice S. J. et al., 2018, ApJ, 865, L3
Quirola-Vásquez J. et al., 2022, A&A, 663, A168
Quirola-Vásquez J. et al., 2023, A&A, 675, A44
Quirola-Vásquez J. et al., 2025, A&A, 695, A279
Ramirez-Ruiz E., Celotti A., Rees M. J., 2002, MNRAS, 337, 1349
Rastinejad J. C. et al., 2025, ApJ, 988, L13
Rhodes L. et al., 2023, MNRAS, 521, 389
Ricci R. et al., 2025, ApJ, 979, L28
Ryan G., van Eerten H., Piro L., Troja E., 2020, ApJ, 896, 166
Saxton R. D., Read A. M., Komossa S., Lira P., Alexander K. D., Wieringa M. H., 2017, A&A, 598, A29
Schulze S. et al., 2021, ApJS, 255, 29
Soderberg A. M. et al., 2008, Nature, 453, 469
Soderberg A. M. et al., 2010, Nature, 463, 513
Srinivasaragavan G. P. et al., 2025, ApJ, 988, L60
Srivastav S. et al., 2025, ApJ, 978, L21
Sun H. et al., 2025, Nat. Astron., 9, 1073
Sun H., Zhang B., Gao H., 2017, ApJ, 835, 7
Tody D., 1986, in Crawford D. L., ed., Proc. SPIE Conf. Ser. Vol. 627, Instrumentation in astronomy VI. SPIE, Tucson, USA, p. 733
van Dalen J. N. D. et al., 2025, ApJ, 982, L47
van der Horst A. J. et al., 2014, MNRAS, 444, 3151
van Dokkum P. G., 2001, PASP, 113, 1420
van Velzen S., Holoien T. W. S., Onori F., Hung T., Arcavi I., 2020, Space Sci. Rev., 216, 124
Virtanen P. et al., 2020, Nat. Methods, 17, 261
Wang J. et al., 2018, ApJ, 867, 147
Wang X.-G., Zhang B., Liang E.-W., Lu R.-J., Lin D.-B., Li J., Li L., 2018, ApJ, 859, 160
Waxman E., Katz B., 2017, in Alsabti A. W., Murdin P., eds, Handbook of Supernovae, Shock Breakout Theory. Springer International Publishing AG, New York, p. 967
Wichern H. C. I., Ravasio M. E., Jonker P. G., Quirola-Vásquez J. A., Levan A. J., Bauer F. E., Kann D. A., 2024, A&A, 690, A101
Wiersema K. et al., 2007, A&A, 464, 529
Wu G.-L. et al., 2025, ApJ, 991, 115
Xinwen S. et al., 2025, ApJ, 990, L29
Xue Y. Q. et al., 2019, Nature, 568, 198
Yadav M. et al., 2025, preprint (arXiv:2505.08781)
Yuan W., Zhang C., Chen Y., Ling Z., 2022, in Bambi C., Sangangelo A., eds, Handbook of X-ray and Gamma-ray Astrophysics. Springer Nature, New York, p. 86
Zhang Y.-Q. et al., 2025, ApJ, 987, L38
Zheng W., Han X., Zhang P., Filippenko A. V. , KAIT GRB team, 2024, GCN Circ., 38136, 1
Zhou H., Li R.-Z., Chen W., Zhao T., Chen X. L., Chatterjee K., Pan H. W., 2024, GCN Circ., 38112, 1

APPENDIX: ADDITIONAL FIGURES AND TABLES

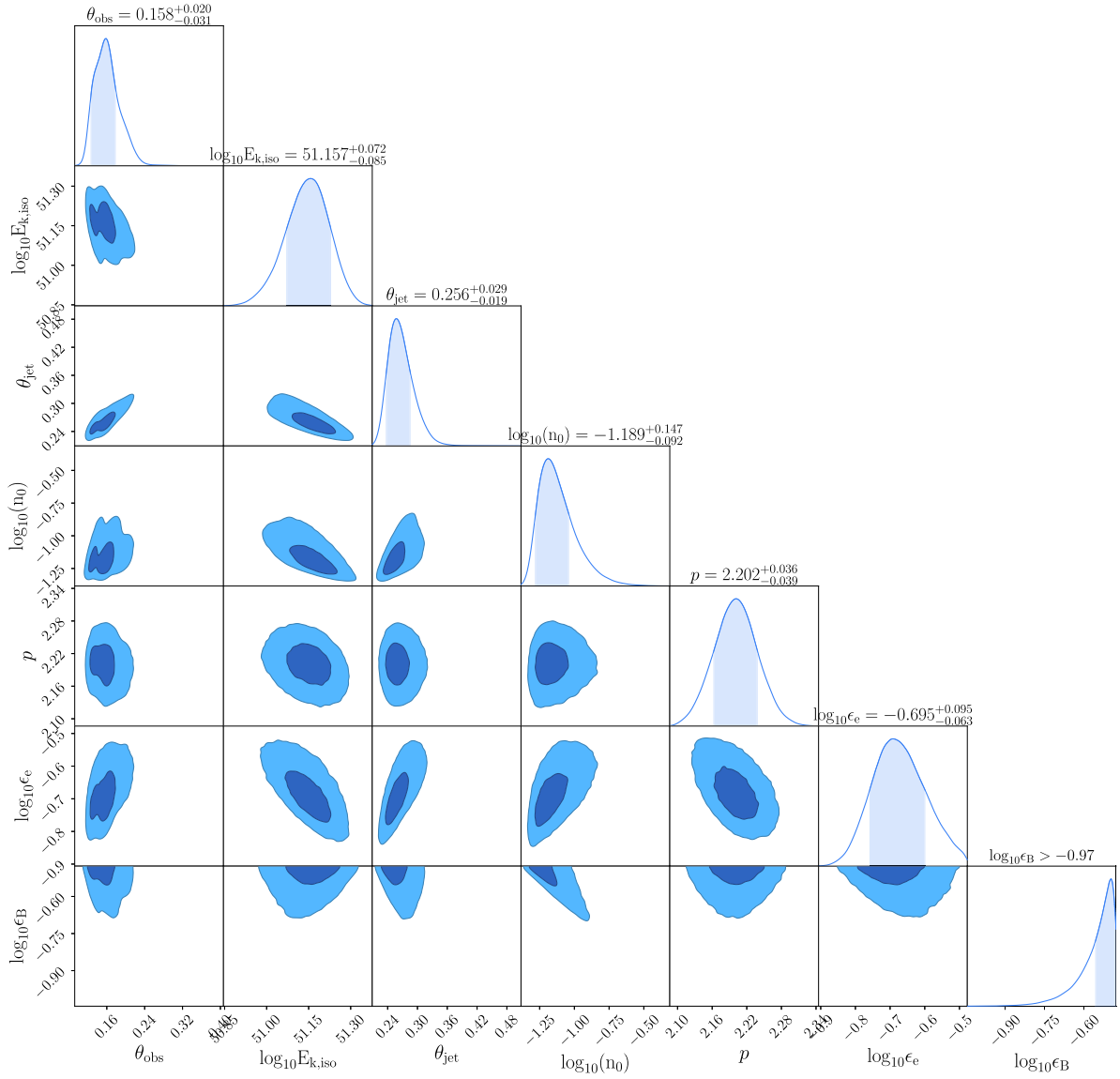

Figure A1. Corner plot for EP241107a.

Table A1. Details of the FXTs used in Fig. 9 from the pre-EP era.

FXT	$L_{x,p}$ (erg s^{-1})	$z_{\rm phot}$	$z_{\rm spec}$	Telescope	Reference
XRT 030206	5×10^{44}	–	0.281 ± 0.003	*XMM–Newton*	D. Eappachen et al. (2024)
XRT 041230	1.1×10^{44}	$0.61^{+0.13}_{-0.17}$	–	*Chandra*	J. Quirola-Vásquez et al. (2022)
XRT 060207*	1.2×10^{46}	–	0.939	*XMM–Newton*	A. Inkenhaag et al. (2024)
XRT 080819	1.5×10^{45}	$0.7^{+0.04}_{-0.10}$	–	*Chandra*	J. Quirola-Vásquez et al. (2022)
XRT 100424†	5×10^{42}	0.13	–	*XMM–Newton*	D. Alp & J. Larsson (2020)
XRT 110621	2×10^{43}	–	0.0928 ± 0.0002	*XMM–Newton*	D. Eappachen et al. (2024)
XRT 151128	3×10^{44}	0.51 ± 0.01	–	*XMM–Newton*	D. Eappachen et al. (2024)
XRT 151219	2×10^{45}	–	0.584 ± 0.009	*XMM–Newton*	D. Eappachen et al. (2024)
XRT 170901	3.7×10^{46}	1.44 ± 0.08	–	*Chandra*	J. Quirola-Vásquez et al. (2023); D. Lin et al. (2022)
XRT 141001/CDF XT1	2.8×10^{47}	$2.76^{+0.21}_{-0.13}$	–	*Chandra*	J. Quirola-Vásquez et al. (2025)
XRT 150322/CDF XT2	1.4×10^{47}	–	3.4598 ± 0.0022	*Chandra*	J. Quirola-Vásquez et al. (2025)
XRT 210423[a]	1×10^{46}	–	1.5082 ± 0.0001	*Chandra*	D. Eappachen et al. (2023); D. Ibrahimzade et al. (2025)
XRO 080109/SN2008D	6.1×10^{43}	–	0.00649 (d=27 Mpc)	*Swift*-XRT	A. M. Soderberg et al. (2008)

Notes. *Considering the galaxy within the 1σ X-ray uncertainty region as the host.
†Based on the combined information of three galaxies/average z; see D. Alp & J. Larsson (2020).
[a]Assuming cNE is the host galaxy of XRT 210423 (D. Eappachen et al. 2023; D. Ibrahimzade et al. 2025).

This paper has been typeset from a TEX/LATEX file prepared by the author.